

# The effects of molecular noise and size control on variability in the budding yeast cell cycle

Stefano Di Talia<sup>1,2</sup>, Jan M. Skotheim<sup>2</sup>, James M. Bean<sup>1</sup>†, Eric D. Siggia<sup>2</sup> & Frederick R. Cross<sup>1</sup>

**Molecular noise in gene expression can generate substantial variability in protein concentration<sup>1</sup>. However, its effect on the precision of a natural eukaryotic circuit such as the control of cell cycle remains unclear. We use single-cell imaging of fluorescently labelled budding yeast to measure times from division to budding (G1) and from budding to the next division. The variability in G1 decreases with the square root of the ploidy through a 1N/2N/4N ploidy series, consistent with simple stochastic models for molecular noise. Also, increasing the gene dosage of G1 cyclins decreases the variability in G1. A new single-cell reporter for cell protein content allows us to determine the contribution to temporal G1 variability of deterministic size control (that is, smaller cells extending G1). Cell size control contributes significantly to G1 variability in daughter cells but not in mother cells. However, even in daughters, size-independent noise is the largest quantitative contributor to G1 variability. Exit of the transcriptional repressor Whi5 from the nucleus partitions G1 into two temporally uncorrelated and functionally distinct steps. The first step, which depends on the G1 cyclin gene *CLN3*, corresponds to noisy size control that extends G1 in small daughters, but is of negligible duration in mothers. The second step, whose variability decreases with increasing *CLN2* gene dosage, is similar in mothers and daughters. This analysis decomposes the regulatory dynamics of the Start transition into two independent modules, a size sensing module and a timing module, each of which is predominantly controlled by a different G1 cyclin.**

In budding yeast (*Saccharomyces cerevisiae*), smaller cells delay the Start transition in late G1, which could imply that cell cycle initiation has a deterministic requirement for a critical size or translation rate<sup>2–5</sup>. However, in apparent contradiction to deterministic models, the timing of G1 in budding yeast shows substantial variability that is independent of cell size<sup>6–9</sup>. Here, we analyse the conflicting roles of deterministic cell size control and molecular noise in gene expression<sup>1,9,10</sup> in generating and controlling cell cycle variability.

We first address the hypothesis that gene expression noise<sup>1</sup> generates significant cell cycle variability. Doubling ploidy doubles the number of all cellular components, but cell volume also doubles, so the average concentrations of cellular components remain constant<sup>11</sup>. If stochastic variation in the numbers of key molecules causes gene expression noise, then doubling their average number along with the ploidy should reduce this noise (expressed as standard deviation divided by the mean) by about  $\sqrt{2}$  (ref. 12). If cell cycle timing is controlled by noisy gene expression, then doubling ploidy should similarly reduce cell cycle variability.

We measured times from cytokinesis to budding (G1) and from budding to cytokinesis in haploids, diploids or tetraploids (mothers and daughters), using time-lapse fluorescence microscopy of strains expressing Myo1 tagged with green fluorescent protein

(Myo1–GFP). Myo1 forms a ring at the new bud neck<sup>13</sup> (concomitant with initiation of DNA replication<sup>2</sup>), which disappears at cytokinesis<sup>13</sup> (Fig. 1). G1 variability is reduced in both mothers and daughters by about the expected factor of  $\sqrt{2}$  for each ploidy doubling (Fig. 1, Supplementary Table 8, Supplementary Fig. 7). Thus molecular noise might be an important source of G1 variability. In marked contrast, variability in the time from budding to cytokinesis is nearly unaffected by ploidy (Supplementary Table 8).

The magnitude and sensitivity to ploidy of G1 noise indicate that the noise might be due to small variable numbers of key regulatory molecules. As G1 cyclins control average G1 duration<sup>14–22</sup> and are expressed at a level of few messenger RNA transcripts per cell<sup>23</sup>, we integrated tandem arrays of the G1 cyclin genes *CLN2* or *CLN3* in haploids. Increasing copy numbers of G1 cyclin genes decreases G1 variability (Fig. 1, Supplementary Table 10), which could help to explain the reduction in variability that is caused by the presence of multiple copies of the entire genome (Fig. 1).

This analysis is based solely on timing; however, cell size has long been proposed as a deterministic regulator of the Start transition<sup>3,11</sup>. To provide a protein-based single cell marker of cell size, we placed the DsRed Red Fluorescent Protein under the control of the promoter of the constitutive, strongly expressed actin (*ACT1*) gene. Assuming that the DsRed transcript accumulates and is translated in parallel with bulk cellular mRNA, then total red fluorescence per cell will reflect total cell protein content. When we quantified total red fluorescence per cell as described<sup>24</sup>, we found exponential growth in single cells (Fig. 2a; Supplementary Information), as deduced previously from pulse-labelling of size-selected populations<sup>25</sup>. The single-cell growth rate  $\alpha$  is moderately variable, but its average agrees well with the bulk culture growth rate (Fig. 2b, Supplementary Table 12). Total red fluorescence scales linearly with ploidy (Supplementary Table 11) and with geometric estimates of cell size. However, using our methods, DsRed fluorescence is a more reliable indicator of cell size than geometric volume estimation (see Supplementary Information). Total red fluorescence for a colony increases exponentially (Fig. 2c), so changes in the microenvironment do not interfere with these measurements. These results support the use of total red fluorescence from *ACT1pr–DsRed* as a single-cell marker for cell size.

Size control at Start would require smaller cells to prolong G1 for growth, thereby linking birth size and G1 duration. Given exponential growth, the size at budding,  $M_{\text{bud}}$ , is related to the size at birth  $M_{\text{birth}}$ , through the amount of time spent in G1 by the simple formula:  $M_{\text{bud}} = M_{\text{birth}} e^{\alpha T_{\text{G1}}}$ , where  $\alpha$  is the growth rate for exponential growth and  $T_{\text{G1}}$  represents the overall duration of G1. This expression yields:  $\alpha T_{\text{G1}} = \ln(M_{\text{bud}}) - \ln(M_{\text{birth}})$ . Plotting correlations between  $\alpha T_{\text{G1}}$  and  $\ln(M_{\text{birth}})$  allows us to distinguish between two classical concepts for G1 control: timers and sizers<sup>26,27</sup>. If G1 duration is under the control of a timer, then  $\alpha T_{\text{G1}}$  will be independent of cell

<sup>1</sup>The Rockefeller University, <sup>2</sup>Center for Studies in Physics and Biology, The Rockefeller University, New York, New York 10021, USA. †Present address: Human Oncology and Pathogenesis Program, Memorial Sloan-Kettering Cancer Center, New York, New York 10021, USA.

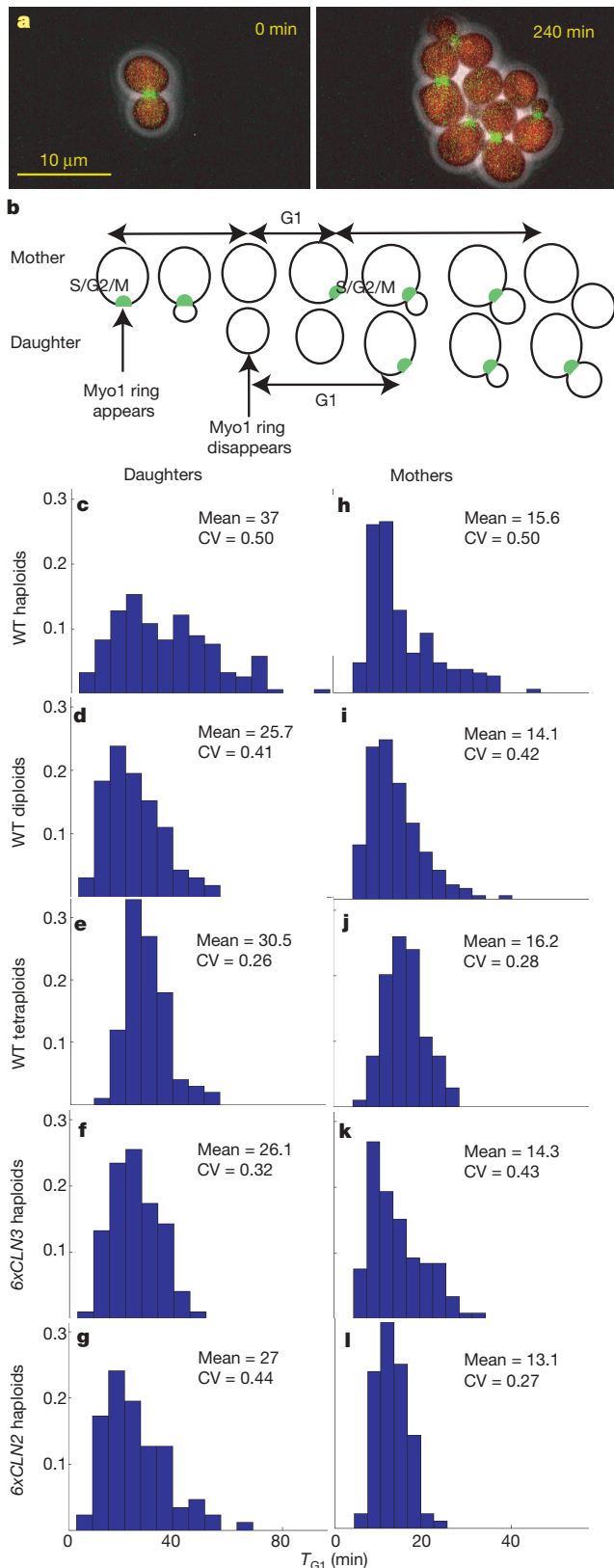


**Figure 1 | Noise in G1 duration is reduced by increased ploidy or increased G1 cyclin gene dosage.** **a**, Composite phase contrast, Myo1-GFP and *ACT1pr*-DsRed images for haploid cells. **b**, Illustration of measured intervals. **c-l**, Frequency histograms ( $n = 87-202$ ) of the duration of G1 for wild-type (WT) haploid (**c**, **h**), diploid (**d**, **i**) and tetraploid (**e**, **j**), haploid  $6\times CLN3$  (**f**, **k**), and haploid  $6\times CLN2$  (**g**, **l**), daughters (**c**, **d**, **e**, **f**, **g**) and mothers (**h**, **i**, **j**, **k**, **l**). Insets: mean and coefficient of variation (CV: s.d./mean, a standardized noise measure).

size at birth, and the slope of the linear fit of the plot of  $\alpha T_{G1}$  against  $\ln(M_{\text{birth}})$  will be 0. By contrast, if G1 is controlled by a sizer, all cells will bud at the same size  $M_{\text{bud}}$ , independent of their size at birth, implying that the slope of the linear fit of  $\alpha T_{G1}$  against  $\ln(M_{\text{birth}})$  will be  $-1$  (ref. 27).

For the following analysis, rigorous statistical testing of fits is described in the Supplementary Information.

Scaled G1 duration in mother cells is essentially independent of cell size (slope  $\approx -0.1$ ), showing that mother G1 is controlled by a timer (Fig. 2d, Supplementary Fig. 9). Daughters, by contrast, show stronger size control (slope  $\approx -0.4$ ). Binning the daughter data (Fig. 2e inset) suggested decomposition into two segments, one for small newborn daughters ( $<67\%$  of the average budding size), in which an efficient sizer was deduced (slope  $\approx -0.7$ ), and a second segment for larger-born daughters, which showed much less dependence on cell size (slope  $\approx -0.3$ ; Fig. 2e). Statistical confidence in this decomposition was limited by the small number of very small daughters obtained; therefore, we employed the genetic method described in ref. 17 to make unusually small wild-type daughter cells by transient expression of conditional *MET3-CLN2* (see Supplementary Information). Inclusion of these data (Fig. 2f) provided strong statistical support for the two-slope model (linear fit:  $P < 0.05$ ; two-slope fit:  $P > 0.7$ ).

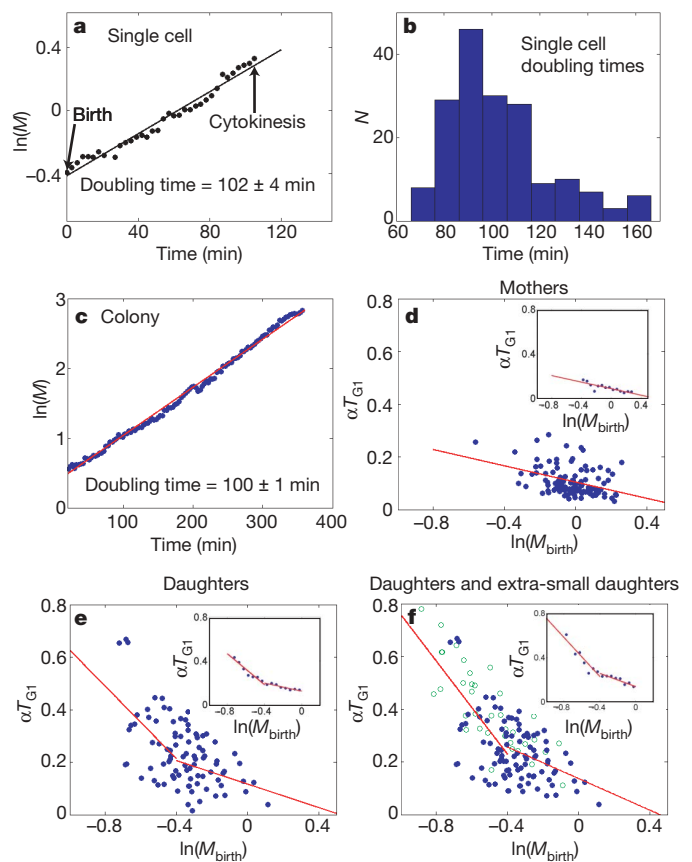


**Figure 2 | The correlation between cell size and G1 duration shows that a noisy size control operates in daughters.** **a**, Logarithm of total DsRed fluorescence ( $M$ ) per cell in a single representative cell from birth to cytokinesis. Doubling time is  $\ln(2)/\alpha$ , where  $\alpha$  is the slope of the linear fit. **b**, Haploid cell doubling time distribution. **c**, Total DsRed fluorescence in an entire colony over time. **d**, **e**, Correlation between  $\alpha T_{G1}$  (growth-rate-standardized time in G1) and  $\ln(M)$  for haploid mothers (**d**) and daughters (**e**) at birth ( $\ln(M_{\text{birth}})$ ). Insets, binned data. **f**, Data from **e** (solid blue dots), supplemented with data from unusually small wild-type haploid daughters (open green circles), generated using essentially the method of ref. 17. For statistical analysis and estimated slopes, see Supplementary Information.

Efficient size control ensures that all cells bud at the same size. As there is variability in cell size at birth, an efficient sizer would ensure that smaller cells spend longer in G1, generating cell-to-cell variability in G1 duration. Measuring individual growth rates and cell sizes allows G1 variability to be decomposed into variability due to size control and a size-independent residual that is attributable to molecular noise. Assuming that G1 duration for an individual cell is the sum of a deterministic function of cell size at birth,  $f(M_{\text{birth}})$ , and a stochastic variable,  $\eta$ , then:  $\alpha T_{G1} = f(M_{\text{birth}}) + \eta$ , where  $f(M_{\text{birth}})$  is obtained empirically by binning data. For a measured distribution of sizes at birth, the variance of  $f(M_{\text{birth}})$  yields the amount of G1 variability that is produced by size control. Size-independent variability is the average distance between a data point and the deterministic  $f(M_{\text{birth}})$ .

This decomposition shows that size-independent (presumably molecular) noise is the leading source of variability in the duration of G1 in both mothers and daughters (Table 1). However, size control accounts for about 30–40% of overall G1 variability in daughters. Consistent with our previous timing analysis, size-independent noise decreases by about a factor of  $\sqrt{2}$  for each ploidy doubling (Table 1; Supplementary Figs 7, 9, 10); thus, ploidy-dependent noise reduction is robust to statistical removal of all detectable size and growth rate effects, indicating that molecular noise is likely to explain size-independent variability. The dosage of the genes for G1 cyclins also decreases size-independent variability; therefore, some of this variability might be attributable to stochastic variation in the expression of G1 cyclins themselves, although other targets cannot be excluded.

We can divide G1 into two steps on the basis of nuclear residence of Whi5<sup>24,28</sup>, which enters the nucleus late in mitosis and exits during G1<sup>28</sup> (Fig. 3a, b). Whi5 represses the transcription of genes that are activated by the SBF/MBF transcription factors<sup>28–30</sup>, including *CLN1* and *CLN2*. Cln3 initiates the inactivation and nuclear exit of Whi5<sup>28–30</sup>. We call the period between cytokinesis and Whi5 exit  $T_1$ , and the period between Whi5 exit and budding  $T_2$ . In mother cells,  $T_1$  is only  $\sim 1$  min (Table 2), so the  $\sim 15$  min length of G1 in mothers is mainly determined by  $T_2$ . By contrast, in daughter cells  $T_1$  and  $T_2$  are about 20 and 17 min, respectively. As  $T_1$  and  $T_2$  are uncorrelated (Fig. 3c), Whi5 exit marks the boundary between two independent steps. For daughters, plotting  $\alpha T_1$ , the time from birth to Whi5 nuclear exit scaled with the growth rate  $\alpha$ , against the logarithm of the size at birth, yields a nearly identical relationship to that for overall G1 duration  $\alpha T_{G1}$  (Figs 2e and 3d, e), shifted down owing to growth during  $T_2$ . The indicated two-slope model fits these data

**Table 1 | Decomposition of G1 variability into a deterministic size control term and a residual attributable to molecular noise**

	G1 noise, birth to budding (coefficient of variation of $\alpha T_{G1}$ )	Noise due to size control (percentage of the total variance of $\alpha T_{G1}$ )	Size and growth rate-independent noise (percentage of the total variance of $\alpha T_{G1}$ )
<b>Daughters</b>			
Wild-type haploids	0.55 ± 0.06	0.31 ± 0.04 (32)	0.45 ± 0.04 (68)
Wild-type diploids	0.42 ± 0.04	0.28 ± 0.03 (45)	0.31 ± 0.03 (55)
Wild-type tetraploids	0.24 ± 0.02	0.15 ± 0.01 (39)	0.19 ± 0.02 (61)
Haploid 6× <i>CLN2</i>	0.48 ± 0.04	0.30 ± 0.03 (39)	0.37 ± 0.03 (61)
Haploid 6× <i>CLN3</i>	0.44 ± 0.04	0.25 ± 0.02 (32)	0.36 ± 0.03 (68)
Haploid 6× <i>CLN3</i> 6× <i>CLN2</i>	0.37 ± 0.03	0.18 ± 0.02 (24)	0.32 ± 0.03 (76)
<b>Mothers</b>			
Wild-type haploids	0.50 ± 0.05	0.20 ± 0.02 (16)	0.46 ± 0.04 (84)
Wild-type diploids	0.39 ± 0.04	0.13 ± 0.01 (11)	0.37 ± 0.04 (89)
Wild-type tetraploids	0.26 ± 0.02	0.09 ± 0.01 (12)	0.24 ± 0.02 (88)
Haploid 6× <i>CLN2</i>	0.33 ± 0.03	0.13 ± 0.01 (16)	0.30 ± 0.03 (84)
Haploid 6× <i>CLN3</i>	0.48 ± 0.05	0.16 ± 0.02 (11)	0.45 ± 0.04 (89)
Haploid 6× <i>CLN3</i> 6× <i>CLN2</i>	0.34 ± 0.03	0.17 ± 0.02 (25)	0.29 ± 0.02 (75)

G1 noise (first column): coefficient of variation of  $\alpha T_{G1}$  ( $\alpha$ , growth rate;  $T_{G1}$ , G1 duration). G1 noise is decomposed into size-dependent and size-independent components (second and third columns); in parentheses, the percentage of the variance of  $\alpha T_{G1}$  accounted for in each column. Noise in  $\alpha T_{G1}$  is the square root of the sum of the squares of the two independent noise contributions.

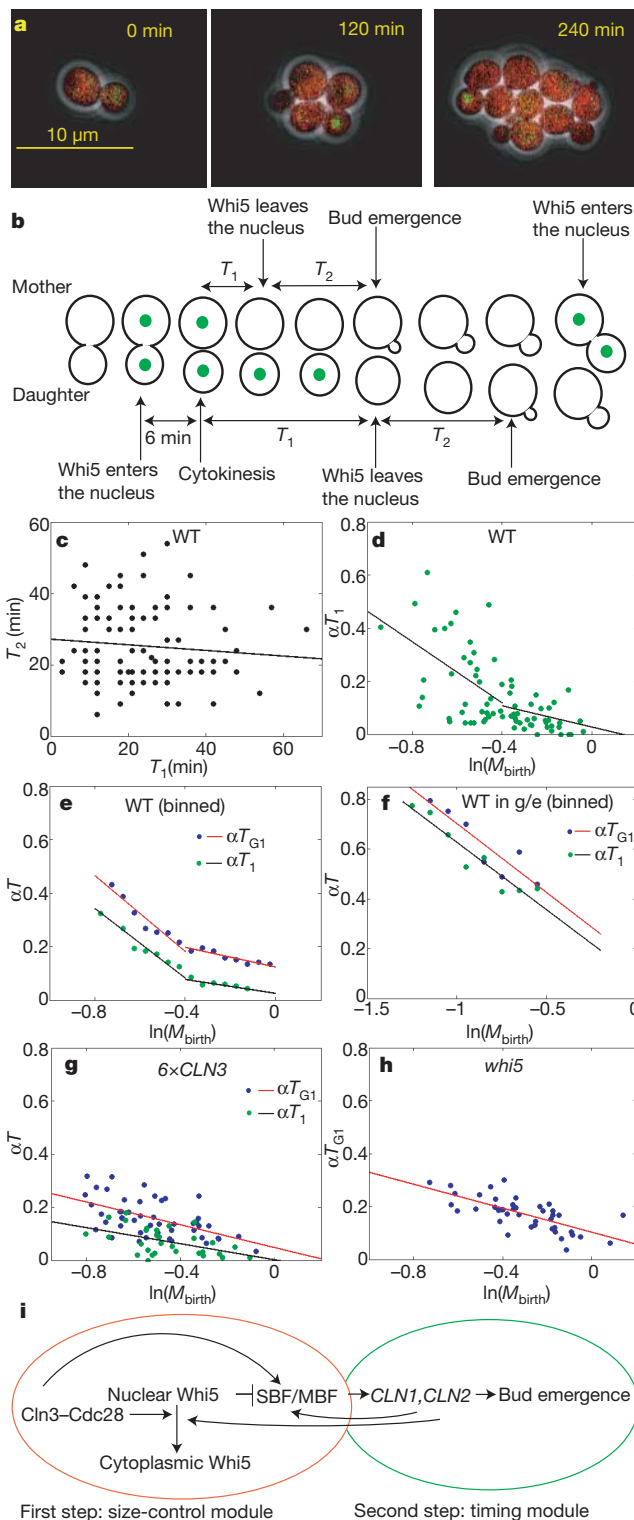


**Figure 3 | The correlation between cell size and the regulation of Whi5 nuclear residence supports decomposition of Start into a size-control module and an independent timing module.** **a**, Composite phase contrast, Whi5–GFP and *ACT1pr*–DsRed images for haploid cells. Whi5–GFP is mostly observed in newborn daughter cells. **b**, Diagram of the measured intervals;  $T_{G1}$  (Fig. 1) is approximately  $T_1 + T_2$ . **c–h** show only data for daughters. **c**,  $T_1$  and  $T_2$  are uncorrelated (correlation coefficient  $-0.1$ ) (data from ref. 24; WT, wild-type). **d**,  $\alpha T_1$  against  $\ln(M_{\text{birth}})$ . **e**, Binned data from Fig. 3d (green points, black line) and Fig. 2e (blue points, red line). **f**, Binned data for  $\alpha T_1$  (green points, black line) and  $\alpha T_{G1}$  (blue points, red line) against  $\ln(M_{\text{birth}})$  for cells grown in glycerol/ethanol (g/e; see also Supplementary Fig. 3). **g**,  $\alpha T_1$  and  $\alpha T_{G1}$  against  $\ln(M_{\text{birth}})$  for 6×*CLN3* cells. **h**,  $\alpha T_{G1}$  against  $\ln(M_{\text{birth}})$  for *whi5* cells. **i**, Model decomposing Start into a size-control module and an independent timing module unaffected by cell size. For statistical analysis, see Supplementary Information.

**Table 2 | Average durations of  $T_1$  and  $T_2$  in different strains**

	Wild type	<i>cln3</i>	$6\times CLN3$	$6\times CLN2$
$T_1$ in daughters	20 ± 1 (157)	30 ± 4 (47)	10 ± 1 (53)	16 ± 1 (80)
$T_1$ in mothers	0.9 ± 0.3 (170)	13 ± 1 (55)	0.7 ± 0.5 (56)	1.1 ± 0.4 (90)
$T_2$ in daughters	17 ± 2 (157)	14 ± 2 (47)	16 ± 1 (53)	11 ± 1 (80)
$T_2$ in mothers	14.7 ± 0.6 (170)	13 ± 1 (55)	13.6 ± 0.8 (56)	12.0 ± 0.6 (90)

$T_1$ , period from cytokinesis to Whi5 nuclear exit;  $T_2$ , period from Whi5 exit to bud emergence (see Fig. 3b). Mean ± s.e.m. in min (number of observations in parentheses).

significantly better than a one-slope model, and the deduced slopes for the Whi5 data and for the total G1 data are similar (see Supplementary Information). Thus, G1 size control is restricted to  $T_1$ , the period of Whi5 nuclear residence.  $T_2$ , the part of G1 after Whi5 exit, is independent of cell size, and similar in mothers and daughters<sup>24</sup> (Table 2).

These observations are robust to changes in nutrient conditions: growth of cells in glycerol/ethanol instead of glucose, resulting in slow growth and generation of very small newborn daughter cells, gave quantitatively similar results (Fig. 3f; see Supplementary Information). As for the small daughters produced by transient *MET3-CLN2* expression (Fig. 2f), the combined data sets for glycerol/ethanol and glucose strongly supported a two-slope model for total daughter G1 and Whi5 nuclear residence times (see Supplementary Information). Even in glycerol/ethanol, mother cells showed little or no size control (Supplementary Fig. 6).

Increasing *CLN3* gene dosage decreases  $T_1$ , whereas increasing *CLN2* gene dosage modestly decreases  $T_2$  (Table 2, see Supplementary Information). Deletion of *CLN3* significantly increased  $T_1$  in both mothers and daughters, so the shortness of  $T_1$  in wild-type mothers is *Cln3*-dependent (Table 2). Efficient size control, indicated by the steep slope for small wild-type daughters, is essentially eliminated by an increase in *CLN3* gene dosage or deletion of *WHI5* (Fig. 3e, g, h).

Changing the copy numbers of *CLN3* as compared with *CLN2* had differential effects on G1 variability in mothers and daughters (Fig. 1). The two-step model explains this, as an increase in *CLN3* copy number should only affect the first step, which is slow in daughters but very rapid in mothers. As, in mothers, G1 is temporally dominated by the second step, mother cell G1 variability is more sensitive to changes in *CLN2* copy number (Fig. 1). Consistent with this idea and with independence of the two steps, combining  $6\times CLN3$  together with  $6\times CLN2$  in one haploid genome resulted in low G1 variability in both mothers and daughters (Table 1, Supplementary Fig. 8).

Therefore, we decompose G1 into two independent steps separated by Whi5 nuclear exit: a size-sensing module and a size-independent timing module. The first step depends on both *Cln3* and cell size, and the second step depends on *Cln2*, but not on cell size or *Cln3* (Fig. 3i). Temporal variability in the first step is due to the natural variability in cell size at birth coupled with size control, as well as molecular noise, possibly due to variability in *CLN3* expression. The duration of the second step is cell-size independent; its variability is affected by the expression of the G1 cyclin *CLN2*, one of the primary final effectors of Start<sup>16–19</sup>. This analysis demonstrates that molecular noise has a role in generating variability in a cellular transition, and provides a precise quantitative framework for the analysis of size control.

## METHODS SUMMARY

**Strain and plasmid constructions.** Standard methods were used throughout. All strains are W303-congenic. All integrated constructs were characterized by Southern blot analysis.

**Time-lapse microscopy.** Cells were prepared for time-lapse microscopy as described<sup>24</sup>. We observed growth of microcolonies with fluorescence time-lapse microscopy at 30 °C using a Leica DMIRE2 inverted microscope with a Ludl motorized XY stage. Images were acquired every 3 min for cells grown in glucose and every 6 min for cells grown in glycerol/ethanol with a Hamamatsu Orca-ER

camera. We used custom Visual Basic software integrated with ImagePro Plus to automate image acquisition and microscope control.

**Image analysis.** Automated image segmentation and fluorescence quantification of yeast grown under time-lapse conditions, and semiautomated assignment of microcolony pedigrees, were performed as described<sup>24</sup>. Budding was scored visually by the appearance of Myo1-GFP at the incipient bud neck, and division by its disappearance, generally with single-frame accuracy. The nuclear residence of Whi5-GFP was scored by visual inspection of composite phase contrast-fluorescent movies. Cell size was measured as the total cell fluorescence from DsRed protein, expressed from the constitutively active *ACT1* promoter. Background was measured as the average fluorescence of unlabelled cells for each movie and subtracted from the measured pixel intensities. To combine data from different experiments, we normalized our measurements of red fluorescence to the average red fluorescence at budding computed for each colony separately. Similar results were obtained by normalizing the size of cells by using the average intensity computed for each colony separately.

**Data analysis.** Time-lapse microscopy data were analysed with custom software written in MATLAB. Binning was performed by marking off nonoverlapping intervals on the horizontal axis, averaging the data in each interval and plotting in the centre of the interval.

**Full Methods** and any associated references are available in the online version of the paper at [www.nature.com/nature](http://www.nature.com/nature).

**Received 12 March; accepted 6 July 2007.**

1. Samoilov, M. S., Price, G. & Arkin, A. P. From fluctuations to phenotypes: the physiology of noise. *Sci. STKE* **366**, re17 (2006).
2. Hartwell, L. H., Culotti, J., Pringle, J. R. & Reid, B. J. Genetic control of the cell division cycle in yeast. *Science* **183**, 46–51 (1974).
3. Hartwell, L. H. & Unger, M. W. Unequal division in *Saccharomyces cerevisiae* and its implications for the control of cell division. *J. Cell Biol.* **75**, 422–435 (1977).
4. Johnston, G. C., Pringle, J. R. & Hartwell, L. H. Coordination of growth with cell division in the yeast *Saccharomyces cerevisiae*. *Exp. Cell Res.* **105**, 79–98 (1977).
5. Moore, S. A. Kinetic evidence for a critical rate of protein synthesis in the *Saccharomyces cerevisiae* yeast cell cycle. *J. Biol. Chem.* **263**, 9674–9681 (1988).
6. Lord, P. G. & Wheals, A. E. Variability in individual cell cycles of *Saccharomyces cerevisiae*. *J. Cell Sci.* **50**, 361–376 (1981).
7. Wheals, A. E. Size control-models of *Saccharomyces cerevisiae* cell proliferation. *Mol. Cell. Biol.* **2**, 361–368 (1982).
8. Lord, P. G. & Wheals, A. E. Rate of cell cycle initiation of yeast cells when cell size is not a rate-determining factor. *J. Cell Sci.* **59**, 183–201 (1983).
9. Nurse, P. Cell cycle control—both deterministic and probabilistic. *Nature* **286**, 9–10 (1980).
10. Spudich, J. L. & Koshland, D. E. Non-genetic individuality: chance in the single cell. *Nature* **262**, 467–471 (1976).
11. Jorgensen, P. & Tyers, M. How cells coordinate growth and division. *Curr. Biol.* **14**, R1014–R1027 (2004).
12. Schroedinger, E. *What is Life?* (Cambridge Univ. Press, Cambridge, 1944).
13. Bi, E. *et al.* Involvement of an actomyosin contractile ring in *Saccharomyces cerevisiae* cytokinesis. *J. Cell Biol.* **142**, 1301–1312 (1998).
14. Cross, F. R. *DAF1*, a mutant gene affecting size control, pheromone arrest, and cell cycle kinetics of *Saccharomyces cerevisiae*. *Mol. Cell. Biol.* **8**, 4675–4684 (1988).
15. Nash, R., Tokiwa, G., Anand, S., Erickson, K. & Futcher, A. B. The WHI1+ gene of *Saccharomyces cerevisiae* tethers cell division to cell size and is a cyclin homolog. *EMBO J.* **7**, 4335–4346 (1988).
16. Tyers, M., Tokiwa, G. & Futcher, B. Comparison of the *Saccharomyces cerevisiae* G1 cyclins: *Cln3* may be an upstream activator of *Cln1*, *Cln2* and other cyclins. *EMBO J.* **12**, 1955–1968 (1993).
17. Dirick, L., Bohm, T. & Nasmyth, K. Roles and regulation of *Cln-Cdc28* kinases at the start of the cell cycle of *Saccharomyces cerevisiae*. *EMBO J.* **14**, 4803–4813 (1995).
18. Stuart, D. & Wittenberg, C. *CLN3*, not positive feedback, determines the timing of *CLN2* transcription in cycling cells. *Genes Dev.* **9**, 2780–2794 (1995).
19. Cross, F. R. Starting the cell cycle: what's the point? *Curr. Opin. Cell Biol.* **7**, 790–797 (1995).
20. McInerney, C. J., Partridge, J. F., Mikesell, G. E., Creemer, D. P. & Breeden, L. L. A novel *Mcm1*-dependent element in the *SWI4*, *CLN3*, *CDC6*, and *CDC47* promoters activates M/G1-specific transcription. *Genes Dev.* **11**, 1277–1288 (1997).
21. Koch, C., Schleiffer, A., Ammerer, G. & Nasmyth, K. Switching transcription on and off during the yeast cell cycle: *Cln/Cdc28* kinases activate bound transcription factor SBF (*Swi4/Swi6*) at start, whereas *Cln/Cdc28* kinases displace it from the promoter in G2. *Genes Dev.* **10**, 129–141 (1996).
22. Wijnen, H., Landman, A. & Futcher, B. The G(1) cyclin *Cln3* promotes cell cycle entry via the transcription factor *Swi6*. *Mol. Cell. Biol.* **22**, 4402–4418 (2002).
23. Holstege, F. C. P. *et al.* Dissecting the regulatory circuitry of a eukaryotic genome. *Cell* **95**, 717–728 (1998).

24. Bean, J. M., Siggia, E. D. & Cross, F. R. Coherence and timing of cell cycle start examined at single-cell resolution. *Mol. Cell* **21**, 3–14 (2006).
25. Elliott, S. G. & McLaughlin, C. S. Rate of macromolecular synthesis through the cell cycle of the yeast *Saccharomyces cerevisiae*. *Proc. Natl Acad. Sci. USA* **75**, 4384–4388 (1978).
26. Donnan, L. & John, P. C. Cell cycle control by timer and sizer in *Chlamydomonas*. *Nature* **304**, 630–633 (1983).
27. Sveczer, A., Novak, B. & Mitchinson, J. M. The size control of fission yeast revisited. *J. Cell Sci.* **109**, 2947–2957 (1996).
28. Costanzo, M. *et al.* CDK activity antagonizes Whi5, an inhibitor of G1/S transcription in yeast. *Cell* **117**, 899–913 (2004).
29. de Bruin, R. A. M., McDonald, W. H., Kalashnikova, T. I., Yates, J. III & Wittenberg, C. Cln3 activates G1-specific transcription via phosphorylation of the SBF bound repressor Whi5. *Cell* **117**, 887–898 (2004).
30. Wittenberg, C. & Reed, S. I. Cell cycle-dependent transcription in yeast: promoters, transcription factors, and transcriptomes. *Oncogene* **24**, 2746–2755 (2005).

**Supplementary Information** is linked to the online version of the paper at [www.nature.com/nature](http://www.nature.com/nature).

**Acknowledgements** We thank J. Haber, E. Bi and the NCRR Yeast Resource Center, University of Washington, for plasmids and strains; P. Nurse and T. Ryan for discussions; and N. Buchler, B. Drapkin, J. Robbins, J. Roberts and J. Widom for comments on the manuscript. This work was supported by the National Institute of Health (J.M.S., E.D.S., F.R.C.), the Howard Hughes Medical Institute (J.M.B.), and the National Science Foundation (E.D.S.).

**Author Contributions** Experimental work by S.D. and J.M.S.; project planning, data analysis and manuscript preparation by all authors.

**Author Information** Reprints and permissions information is available at [www.nature.com/reprints](http://www.nature.com/reprints). The authors declare no competing financial interests. Correspondence and requests for materials should be addressed to F.R.C. ([fcross@mail.rockefeller.edu](mailto:fcross@mail.rockefeller.edu)).

## METHODS

**Strain and plasmid constructions.** Standard methods were used throughout. All strains are of the W303 background. The plasmid pSD03 (pRS403-*CLN2*) was obtained by cloning the *SmaI*-*SfoI* fragment containing *CLN2* genomic DNA obtained from the *Yep24-CLN2* 2 $\mu$  plasmid (J. McKinney, unpublished data) at the *SmaI* site in pRS403. The *CLN2* genomic fragment started 1.4 kb upstream of the *CLN2* open reading frame and ended about 8 kb downstream. A homologous recombination pop-out of the Ty1 (retrotransposon) downstream of *CLN2* was found in the original *Yep24-CLN2* 2 $\mu$  plasmid. pSD03 was integrated at the *HIS3* locus by *BglII* digestion. Strain SD27-1-1A was confirmed by Southern blot analysis to have five duplicative integrations of pSD03. The plasmid pJB06T (pRS404-*ACT1pr-DSRED*) was obtained as follows. The *ACT1pr* (~500 bp upstream of the *ACT1* open reading frame) was inserted into pTY24 (obtained from NCRR Yeast Resource Center, University of Washington) just upstream of *DSRED* coding sequence. The *BamHI*-*BglII* fragment containing *ACT1pr-DSRED* was then inserted at the *BamHI* site in pRS404. Plasmid pSD02 (pRS406-*ACT1pr-DSRED*) was obtained by cloning the *BglII* fragment containing *ACT1pr-DSRED* obtained from pJB06T into the *BglII* fragment containing *URA3* obtained from pRS406. pSD02 was integrated at the *URA3* locus by *NcoI* digestion. Strain SD20-1A was confirmed by Southern blot analysis to have two duplicative integrations of pSD02. All the other strains that carry pSD02 were obtained by crosses with SD20-1A or with strains derived from it so they also have two duplicative integrations of pSD02. We observed that strains transformed with one copy of pJB06T or two copies of pSD02 behave identically with the only difference that the average intensity of the second reporter is about twice as large as the average intensity of the first one, as expected by difference in copy number. A *MYO1-GFP* strain<sup>13</sup> was backcrossed at least five times to W303 to obtain the strains used in this paper.

**Time-lapse microscopy.** Cells were prepared for microscopy and time-lapse microscopy as described<sup>24</sup>. We observed growth of microcolonies with fluorescence time-lapse microscopy at 30 °C using a Leica DMIRE2 inverted microscope with a Ludl motorized XY stage. Images were acquired every 3 min for cells grown in glucose and every 6 min for cells grown in glycerol/ethanol with a

Hamamatsu Orca-ER camera. We used custom Visual Basic software integrated with ImagePro Plus to automate image acquisition and microscope control.

**Image analysis.** Automated image segmentation and fluorescence quantification of yeast grown under time-lapse conditions, and semiautomated assignment of microcolony pedigrees, were performed as described<sup>24</sup>. Budding and division were scored by visual inspection for the appearance and disappearance of the Myo1-GFP signal, respectively. Detection of the appearance of the Myo1-GFP signal was facilitated by thresholding the images and plotting the pixels above threshold on a linear grey scale. The nuclear residence of Whi5-GFP was scored by visual inspection of composite phase contrast-fluorescent movies and confirmed by the method described for Myo1-GFP detection. Scoring of cell cycle events by monitoring the localization of Myo1-GFP and Whi5-GFP is much faster than detection of newly synthesized, cell-cycle-regulated fluorescent proteins and allows a much higher temporal resolution. Cell size was measured as the total cell fluorescence from DsRed protein, expressed from the constitutively active *ACT1* promoter. Background was measured as the average fluorescence of unlabelled cells for each movie and subtracted from the measured pixel intensities. The measurement of cell size at given time points displayed an appreciable variability, probably due to experimental noise in the imaging and errors in the segmentation of cell bodies. The effect of this noise on size measurements was efficiently averaged out by extracting cell size at a given time point from the least-square fit to exponential growth. The average fluorescent intensity of identical strains imaged on different days and with different fluorescent lamps displayed variability much larger than natural variability among cells in the same colony. To combine data from different experiments we normalized our measurements of cell size to the average size at budding computed for each colony separately. Similar results were obtained by normalizing the size of cells by using the average intensity computed for each colony separately.

**Data analysis.** We analysed time-lapse microscopy timing and fluorescent data with custom software written in MATLAB. Binning was performed as follows: multiple points were placed in bins and averaged. The averages and the values of the centre of the bin were then plotted. Similar results to that obtained by binning the data were obtained by smoothing the data with a moving average.